(This is a sample cover image for this issue. The actual cover is not yet available at this time.)

Remote Sensing of Environment 125 (2012) 134–146

Contents lists available at SciVerse ScienceDirect

Remote Sensing of Environment

journal homepage: www.elsevier.com/locate/rse

Linking fish assemblages and spatiotemporal thermal heterogeneity in a river-floodplain landscape using high-resolution airborne thermal infrared remote sensing and in-situ measurements

Diego Tonolla [a,b,*], Christian Wolter [a], Thomas Ruhtz [c], Klement Tockner [a,b]

[a] IGB, Leibniz-Institute of Freshwater Ecology and Inland Fisheries, Müggelseedamm 310, 12587 Berlin, Germany
[b] Institute of Biology, Freie Universität Berlin, Takustrasse 3, 14195 Berlin, Germany
[c] Institute of Space Sciences, Freie Universität Berlin, Carl-Heinrich-Becker-Weg 6–10, 12165 Berlin, Germany

ARTICLE INFO

Article history:
Received 6 January 2012
Received in revised form 18 July 2012
Accepted 20 July 2012
Available online xxxx

Keywords:
Thermal infrared imagery
TIR
Temperature patterns
Fish distribution
Lowland river
River landscape
Floodplain
Shifting habitat mosaic
River ecosystem
Oder River
Flow regime

ABSTRACT

River floodplains are heterogeneous landscapes composed of a mosaic of aquatic and terrestrial habitats. While flow has frequently been considered as a master variable that controls aquatic biodiversity and species behavior in river floodplains, little is known about thermal heterogeneity and its effect on aquatic biota in complex landscapes. However, quantifying thermal patch dynamics at the river floodplain scale remains a challenging task. In this study, we applied airborne thermal infrared (TIR) imagery to characterize spatial thermal heterogeneity under high (March 2010) and mean (July 2010) flow conditions in a 347.5 ha lowland river floodplain (Oder River, Germany). Concurrently, we electro-fished all major floodplain water bodies (main channel, side channel, and permanently connected ponds) to identify the composition of associated fish assemblages. In addition, we deployed temperature loggers from March to July across the entire range of floodplain water bodies to assess seasonal temperature patterns at 20 min intervals. Under both flow conditions, the TIR imagery revealed a complex mosaic of thermal patches across the floodplain. Cumulative degree-days and average and maximum temperatures were the main variables that thermally differentiated individual water bodies. The water body types delineated based on spatial and seasonal thermal signatures also contained distinct fish assemblages. Distinct temperature gradients at the floodplain scale and both within and across distinct water body types were resolved with airborne thermal data, providing a fully spatial and concurrently available temperature mosaic. A delay in response of fish distribution to a strong thermal gradient recorded in spring, that has never been predicted or observed elsewhere, could be assessed by the use of TIR imagery. This study demonstrates the potential of airborne remotely sensed TIR imagery as a non-invasive method for detecting and quantifying spatial heterogeneity and ecologically relevant temperature gradients in complex landscapes, thereby facilitating the "up-scaling" of ecosystem processes to the landscape scale and expanding current understanding of fish behavior.

1. Introduction

High-resolution satellite and airborne remote sensing are rapidly evolving tools for accurately quantifying the structure and dynamics of complex river landscapes, a prerequisite for improving our understanding of ecosystem processes and biodiversity at various scales (Goetz et al., 2008; Johnson & Host, 2010; Marcus & Fonstad, 2008; Mertes, 2002; and references therein). Remote sensing sensors include (i) multispectral imagers (e.g., CASI, GeoEye, Ikonos, QuickBird) for quantifying suspended sediment concentrations, chlorophyll, turbidity, and water depth; (ii) laser scanners (e.g., LIDAR) for the generation of digital topographic maps and for water surface classification and delineation; and (iii) thermal infrared cameras (e.g., FLIR) for measuring surface temperatures.

River floodplains are heterogeneous landscapes composed of a shifting mosaic of interconnected aquatic and terrestrial habitats. The composition, configuration and degree of hydrological connectivity of these habitats determine biodiversity and ecosystem processes (Tockner & Stanford, 2002; Ward, 1998). Moreover, they determine fish assemblage diversity (Schomaker & Wolter, 2011; Van den Brink et al., 1996; Welcomme, 1979), fish reproduction and juvenile recruitment (Bischoff, 2002; Bischoff & Wolter, 2001; Grift et al., 2003), as well as fish production (Welcomme, 1979).

Temperature is a master variable that influences physical, chemical, biological, and ecological processes in aquatic ecosystems (Caissie, 2006; Magnuson et al., 1979; Webb, 1996; and references therein), triggers the dispersal of ectothermic organisms such as fish (Buisson et al.,

* Corresponding author at: IGB, Leibniz-Institute of Freshwater Ecology and Inland Fisheries, Müggelseedamm 310, 12587 Berlin, Germany. Tel.: +49 30 64181 709; fax: +49 30 64181 600.
E-mail address: tonolla@igb-berlin.de (D. Tonolla).

0034-4257/$ – see front matter © 2012 Elsevier Inc. All rights reserved.
http://dx.doi.org/10.1016/j.rse.2012.07.014

2008; Tiffan et al., 2009), and determines the behavior and survival of fish (Buisson et al., 2008; McCullough et al., 2009; Pörtner & Farrell, 2008). In complex river floodplain mosaics temperature is inherently highly variable in space and time (Caissie, 2006; Tonolla et al., 2010), and, therefore, difficult to quantify using conventional in-situ methods.

Thermal infrared (TIR) imagery has been successfully used to determine the spatial heterogeneity of stream and river temperatures (Cristea & Burges, 2009; Faux et al., 2001; Torgersen et al., 2001), to identify areas of groundwater-surface water interactions (Deitchman & Loheide, 2009; Loheide & Gorelick, 2006), to determine thermal mixing dynamics and velocity fields (Andrews et al., 2011; Cardenas et al., 2011), to calibrate and validate stream temperature models (Cristea & Burges, 2009; Loheide & Gorelick, 2006), and to monitor the success of restoration projects (Loheide & Gorelick, 2006; Shuman & Ambrose, 2003). Moreover, TIR imagery has been employed to identify warm and cold-water refuges that are critical for the survival of many biota, including fish (Madej et al., 2006; Torgersen et al., 1999, 2006), as well as for linking thermal with microbial distribution patterns (Dunckel et al., 2009). However, up to now, most studies have used TIR imagery at the micro- and meso-habitat level, or for mapping the temperature along river corridors. So far, we are only aware of two studies that have used TIR imagery to quantify thermal heterogeneity at the landscape scale (Alpine landscapes: Scherrer & Körner, 2010; braided river floodplains: Tonolla et al., 2010).

The main aim of the present study was to quantify the spatiotemporal heterogeneity of temperature (during two different flow conditions) at the river-floodplain scale by applying aerial TIR imagery together with in-situ temperature recording using conventional loggers. The second aim was to evaluate the potential link between thermal heterogeneity and the structure of fish assemblages at the river floodplain scale. We hypothesized that ectothermic fish strongly respond to high temperatures, especially in spring. It was further hypothesized that given a strong correspondence between in situ measurements and TIR imagery, the latter can be used to predict spatiotemporal heterogeneity in fish assemblage structure.

2. Material and methods

2.1. Experimental design

Thermal long-wavelength infrared (LWIR) and visible spectrum images were remotely collected during two low altitude flights (~300 m agl) to spatially map continuous patterns of surface temperature and water extent under two different flow conditions in a dynamic river floodplain (area: 347.5 ha) along the lowland Oder River (Fig. 1). Concurrently, all major river and floodplain water bodies were electro-fished to assess the composition of fish assemblages. In addition, temperature loggers were deployed from March to July in various water bodies, distributed across the entire floodplain, to assess temperature at 20 min intervals (Fig. 1).

2.2. Study area

The 854 km long Oder River drains a catchment of 118,861 km^2. The average discharge at the mouth is 522 m^3 s^{-1} (LUABB, 1998). Detailed information on the Oder catchment can be found elsewhere (Dohle et al., 1999; Pusch et al., 2009). The study area was located on the German bank between river-km 603.8 and 608 (52°30′31″ N, 14°36′30″ E) at 15 m asl. The floodplain covered 347.5 ha with a maximum width of 1.1 km (Fig. 1). The floodplain is bordered by dikes. The main channel is regulated by groynes and its banks are fortified with rip-rap. The floodplain contains a set of water bodies that differ in the degree of hydrological connectivity with the main channel. In the study area, the main river channel exhibits a mean annual water temperature of 11.4 °C (range: −0.1 to 25.8 °C), a mean annual discharge of 240 m^3 s^{-1} (range: 96.3 to 476 m^3 s^{-1}), and a mean annual

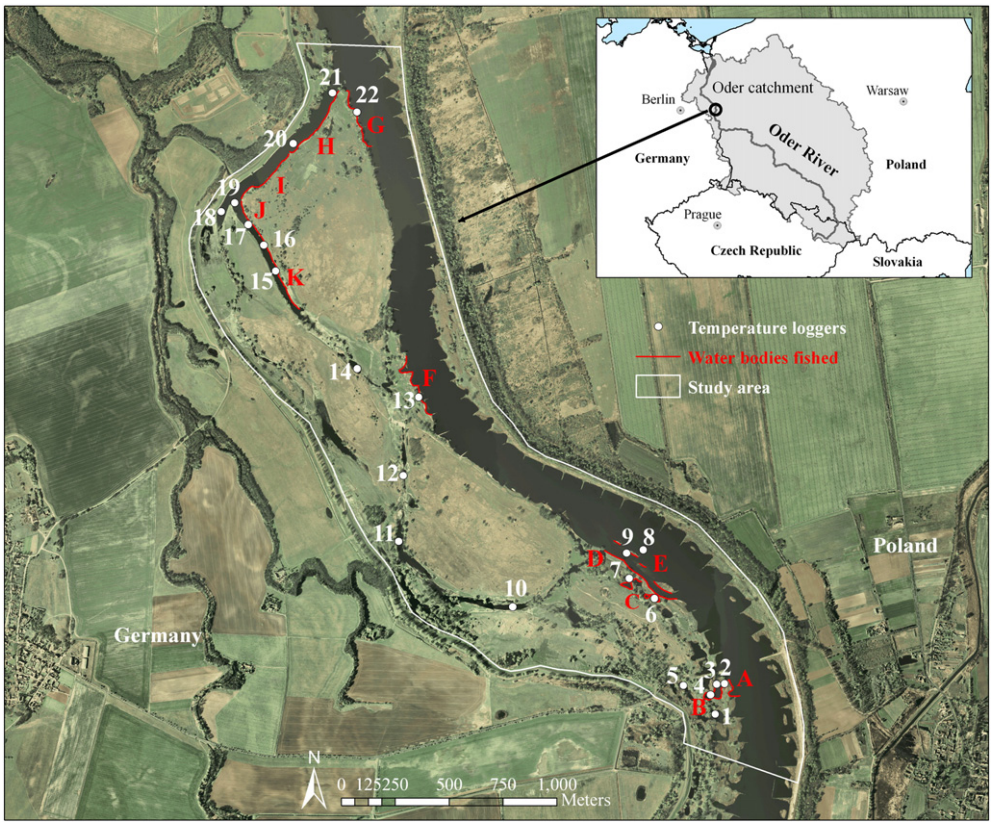

Fig. 1. Study area, water bodies fished (A, D–G: main channel; B, C: permanently connected pond; H–K: side channel) and locations of in-situ temperature loggers in the River Oder floodplain at "Reitwein" (map data source: 20 cm resolution digital orthophoto, Geodata infrastructure Berlin/Brandenburg, Germany).

water depth of 213 cm (range: 116 to 320 cm) (Water and Navigation Authority Eberswalde, 2008, unpublished).

2.3. Airborne remote sensing surveys

2.3.1. Setting for airborne remote sensing image collection

The main channel and the fringing floodplain were mapped on two days with clear skies from early to mid-afternoon (Table 1). At this time of the day the relative humidity is normally constant and low, and it coincides with the maximum daily temperature. Flights were scheduled for the end of March (high flow) and mid-July 2010 (mean flow) (Table 1). On each date, 15 parallel flight lines with an average length of 8 km were required in order to cover the entire study area. Remotely sensed images were collected over a period of approximately 80 min during each flight period (Table 1).

The images were collected with an airborne research platform (modified Cessna 207 T, owned by the Institute of Space Science of the Freie Universität, Berlin, Germany), flying at a consistent altitude (~300 m agl) and at constant speed (~200 km h^{-1}). The Cessna was equipped with an internally calibrated LWIR (7.5–14 μm) camera (VarioCAM high resolution head, InfraTec, Dresden, Germany) and a visible near-infrared (VNIR, 0.4–1.0 μm) compact airborne spectrographic imager (CASI 550, Itres Research Limited, Calgary, Canada, owned by ARSF, Nerc, UK). The two sensors were aligned and mounted in a vertical (nadir) position on a real-time three-axis hydraulically stabilized platform (GSM3000, Zeiss, Jena, Germany). This setting minimized image distortions associated with aircraft motion, side winds and air turbulence (Supplementary Data A).

Each LWIR and VNIR image frame was digitally collected and stored directly in-flight from the sensors on an on-board computer at a rate of 500 and 75 ms, respectively. Finally, the images were tagged with the acquisition time as well as the position and orientation data provided by an inertial navigation system (Aerocontrol, IGI Airborne Systems, Kreuztal, Germany), which combines a fiber-optic gyro-based inertial measurements unit (IMU-IId) and an airborne computer unit with an integrated 12-channel L1/L2 GPS receiver for the precise determination of the absolute position and the attitude of the airborne sensors.

The LWIR images were used to provide surface temperature data (T_r: radiant temperature; radiant temperature is equivalent to the emitted energy of an object) at a high spatial resolution (0.25 × 0.25 m nominal ground pixel size), whereas images within the visible spectrum (derived from the VNIR images, see Section 2.3.3.) were used to provide a visual overview of the study area at high and mean flow conditions, as well as to help delineate the floodplain water bodies in the LWIR images. The post-processed pixel size of the LWIR and the VNIR was 0.5 × 0.5 m and 1 × 1 m, respectively. Additional information on the sensors and their setting is provided in Supplementary Data A.

Table 1
Characterization of the hydrological and meteorological conditions during the remote sensing surveys (values averaged over the entire flying period).

Variables	25 March (high flow)	14 July (mean flow)
Time of remote sensing survey[a]	13:40–15:00	11:50–13:10
Discharge (m^3 s^{-1})[b]	476.0	204.7
Flow depth (cm)[b]	334.0	203.3
Water temperature (°C)[b]	8.1	25.8
Rel. humidity (%)[c]	44.5	51.0
Wind velocity (m s^{-1})[c]	4.4	2.5
Air temperature (°C)[c]	19.9	29.0
Cloud cover (% clouded)[c]	0.05	0.15

[a] Flight start and end times (UTC, hh:min).
[b] Discharge recorded at the gauging station "Eisenhüttenstadt" (river-km 554.1); flow depth and water temperature recorded at the gauging station "Frankfurt/Oder" (river-km 585.3). Data source: Water and Navigation Authority Eberswalde.
[c] Recorded from a meteorological station near the village "Manschnow" (an approximate aerial distance of 7 km downstream from the study area). Data source: http://www.wetteronline.de/.

2.3.2. LWIR image processing

The individual LWIR image frames (n = 1540 (spring) and n = 1250 (summer)) were digitally stored with each pixel containing the radiance values measured by the detector. Sensor internal calibration software converted the thermal radiance values to radiant temperature values (T_r) using Planck's radiation law and sensor calibration curves by considering the emissivity of water, atmospheric transmissivity and ambient background reflections (Supplementary Data B). The LWIR images were processed assuming a TIR emissivity of water of 0.98 (0.983 at a zenith angle of 0° and thermal band of 8–13 μm; Cuenca & Sobrino, 2004).

The main interest of this study was to quantify the relative temperature patterns at the floodplain scale rather than derive absolute temperature values at specific points. The potential inaccuracies of thermal remote sensing for absolute temperature measurements have to be balanced with the pixel resolution in favor of the large-scale data provided by such techniques (Marcus & Fonstad, 2008). The LWIR sensor had a high thermal sensitivity allowing for the detection of relative temperature differences of <0.06 K (manufacturer's accuracy specification). We estimated the potential errors of the LWIR images collected because thermal remote sensing is not without shortcomings (e.g., Handcock et al., 2012, 2006; Kay et al., 2005; Torgersen et al., 2001) and because the remote thermal surveys covered a large area with probable changes in atmospheric and ambient conditions (Supplementary Data B). In-situ recording with temperature loggers (see Section 2.4.1.) showed an average water temperature change throughout the duration of the flight of 0.4 ± 0.2 °C (both dates). Thus, the LWIR images were not corrected for temperature changes due to elapsing time. The major source of error for absolute temperature recording was thermal stratification of water, which was detected during the summer (mean flow) survey in all of the measured water bodies, except in the main channel (Supplementary Data B). Thermal stratification was absent during the spring (high flow) survey. During stratification in the summer, the temperature cannot be considered as being indicative of the overall water column temperature or of cold-water areas near the bottom.

2.3.3. LWIR and VNIR image post-processing workflow

In order to generate single LWIR-image mosaics of the entire floodplain, three main post-processing steps were required. First, T_r values were extracted as ASCII files using the IR analyzing software IRBIS 3 professional (InfraTec, Dresden, Germany) and converted into floating point rasters in ArcGIS 9.3 (ESRI, Redlands, CA, USA). Second, each raster image frame was manually scaled, rotated and individually aligned using the navigation data as a reference. Third, multiple overlapping raster image frames were manually assembled and registered in a final single raster mosaic using the nearest neighbor function to conserve the original values.

The processing chain of the VNIR instrumentation was written in IDL 7.1 (ITT-VIS, Boulder, CO, USA) by T. Ruhtz et al. (unpublished) using navigation data to geocorrect the VNIR image strips (which corresponded to the flight lines). The images were not corrected for atmospheric effects. The geocorrected image strips were then saved as RGB images (only three spectral bands were selected to generate the RGB images, no further spectral analyses were performed; Supplementary Data A) and stitched together to generate a single mosaic of the entire floodplain. Finally, the LWIR and RGB mosaics were georeferenced using a 20 cm resolution digital orthophoto (Geodata infrastructure Berlin/Brandenburg, Germany) as a reference.

Missing parts in the final mosaics were due to sensor and/or GPS malfunctions during the survey. Visible striped patterns in the mosaics were the result of exposure and illumination artifacts associated with image joining and atmospheric effects but they did not

significantly affect the TIR imagery (temperature differences: 0.1—0.3 °C).

2.4. Field surveys

2.4.1. Kinetic water temperature

The kinetic water temperature (T_k; kinetic temperature is the contact heat energy of an object) was continuously recorded at 20 min intervals using temperature loggers (TR model 12 bit, AMIRIX Systems Inc., Halifax, NS, Canada; temperature range −5 to 40 °C, resolution 0.015 °C, accuracy ± 0.1 °C, manufacturer's specification). In total, 30 loggers were used to cover all representative water bodies (main channel, side channel, permanently connected ponds, and ponds that became isolated at low-mean flow; Fig. 1). Recording period lasted from March 24 at 17:00 until July 21 at 23:40 2010. Prior to and after the sampling period, the loggers were calibrated in a temperature-controlled water bath for their working range (maximum error: 0.05 °C). A handheld GPS receiver (GPSmap 60CS, Garmin international, Inc., Olathe, KS; average accuracy during the surveys 3.3 ± 1.8 m) was used to determine the position of the loggers. The loggers were placed in a water depth of 0.2—0.5 m to measure the surface water temperature, which was estimated by means of IR thermography (thermal radiation emitted from the upper ~50 μm surface; Lillesand et al., 2008). In the main channel, two loggers were attached to buoys marking the fairway for inland vessels. These were the only possible logger positions in the main-channel thalweg. Eight loggers were lost due to either a major flood event (maximum: 1950 $m^3 s^{-1}$, 28 May 2010) or to human intervention. Another two loggers (# 1 and 12, Fig. 1) went dry for a maximum of 70 days, resulting in approximately 60% of missing data. The data from these two loggers and from another that was stolen from the main-channel thalweg (# 8, Fig. 1) could only be used to cross-check the accuracy of the T_r derived from the LWIR mosaics (Supplementary Data C) and were excluded from further analyses.

The T_k values from the gauging station "Frankfurt/Oder", located at river-km 585.3, were used to characterize the temperature variation in the main-channel thalweg. A preliminary Spearman's rank correlation analysis revealed a strong correlation between the T_k from the available data of logger # 8 in the main-channel thalweg and the gauging station ($r = 0.99$, $p < 0.001$, $n = 683$, R-project, version 2.9.2). Therefore, further temperature analyses were performed using the data of the remaining 19 loggers and from the gauging station (Fig. 1).

Recording the T_k enabled quantifying seasonal temperature patterns. Furthermore, the T_k values were used to cross-check the accuracy of the T_r derived from the LWIR mosaics (Supplementary Data C). Relative temperature values were used for further analysis because this study aimed to analyze patterns of temperature distribution in floodplain habitats rather than absolute temperatures, which were always well above and below the critical lower and upper temperature thresholds for fish, respectively.

2.4.2. Fish sampling and characterization of the water bodies fished

In parallel to the remote sensing surveys, fish were sampled from 10:00 to 19:00, with a break during the flights. Eleven representative floodplain water bodies (main channel, side channel, and permanently connected ponds; Fig. 1) were sampled by two teams along the banks using two 7 kW and 8 kW DC electro-fishing gears (Types FEG 7000 and FEG 8000, EFKO Fischfanggeräte, Leutkirch, Germany) and a handheld ring anode of 0.4 m diameter each. This type of equipment allows a representative sampling of fish ≥ 5 cm in total length. Therefore, smaller fish were excluded from further analyses. All water bodies were single-pass electro-fished from a boat without stop nets along a bank length of between 70 and 480 m depending on the size of the water body at high and mean flow. Stunned fish were immediately collected by a second operator using a separate dip net. All of the fish caught were identified to species level, counted, measured (total length), and returned to the water. During the two fish surveys, the following environmental variables were recorded at each site: dissolved oxygen concentration, pH, and water surface temperature, measured using handheld multi-parameter water quality meters (U-10, Horiba Ltd., Kyoto, Japan; temperature accuracy ± 0.3 °C, dissolved O_2 accuracy ± 0.1 mg L^{-1}, pH accuracy ± 0.05, manufacturer's specifications), and substrate type, submerged and emerged macrophytes, woody debris, water depth, and type of embankment were visually estimated (Table 2). The water velocity along the banks during electro-fishing was observed as being at similarly low level in all of the water bodies sampled.

2.5. Data analysis

2.5.1. Spatial patterns of surface temperature

At the floodplain scale, the spatial thermal patterns were first investigated using visualization techniques and then subsequently through appropriate data analyses. First, the T_r of each pixel falling in the study area was extracted and used to quantify the T_r pixel frequency distribution. The emissivity of the materials targeted in the floodplain (e.g., grass, shrubs, mature vegetation, sand) had theoretical emissivity values close to that of water (0.96—0.98, at a zenith angle of

Table 2
Environmental characteristics of the 11 water bodies fished (A, D–G: main channel; B, C: permanently connected pond; H–K: side channel; see Fig. 1). Unless stated otherwise, the classes were the same during both field surveys.

		Water bodies fished										
Sampling day	Variable	A	B	C	D	E	F	G	H	I	J	K
25 March (high flow) & 14 July (mean flow)	Sand[a]	3	2	2	3	3	3	3	3	3	3	3
	Silt[a]	2	3	3	1	1	1	1	2	2	2	2
	Organic substrate[a]	1	3	3	1	1	2	2	3	3	3	3
	Submerged macrophytes[b]	1	2	2	2	2	2	1	1	2	2	2
	Emerged macrophytes[b]	2	2	2	1	2	1	1	1	1	1	1
	Woody debris[b]	1	2	2	1	1	1	1	2	2	2	2
	Water depth[c]	3	2	2[d]	3	3	3	3	3	3	2	2
	Embankment[a]	1	1	1	1	1	3	3	2	2	1	1
25 March (high flow)	T_k (°C)	8.8	9.2	9.0	7.9	7.9	8.7	8.1	8.8	9.8	10.2	14.0
	Dissolved O_2 (mg L^{-1})	12.1	12.0	11.5	10.8	10.8	12.5	12.2	15.3	15.5	16.5	19.1
	Water pH	9.6	9.3	9.3	9.3	9.3	9.4	9.3	9.3	9.3	9.5	9.7
14 July (mean flow)	T_k (°C)	26.0	29.2	29.4	26.8	26.8	26.9	26.7	28.0	28.8	30.5	30.1
	Dissolved O_2 (mg L^{-1})	8.1	12.9	13.5	9.8	9.8	13.2	10.4	9.8	10.2	12.0	12.2
	pH	8.7	8.9	8.9	8.9	8.9	8.4	8.3	8.3	8.3	8.4	8.3

[a] 1: absent/insignificant; 2: moderate; 3: dominant.
[b] 1: cover ≤ 10%; 2: cover > 10%.
[c] 1: 0.5–1 m; 2: 1–2 m; 3: 2–5 m.
[d] Class 1 on 14 July.

0° and a thermal band of 8–14 μm; Cuenca & Sobrino, 2004; MODIS, 2011). Second, a side channel (water bodies H–K, Fig. 1) was subsequently selected and analyzed further. Then, polygons were generated in ArcGIS 9.3, and T_r values of each pixel falling in these polygons (for advantages of this technique see Supplementary Data B) were then extracted. We calculated: (i) total number of pixels, (ii) minimum T_r, (iii) maximum T_r, (iv) average T_r, and (v) T_r amplitude (i.e., difference between maximum and minimum T_r). Temperature categories with fewer than 10 pixels were omitted. Third, T_r gradients were analyzed by extracting the T_r values of each pixel spaced by 0.5 m falling in the thalweg of a side channel. Fourth, polygons (width: 3 m) were generated for each water body, representing the effective electric field, i.e. the area fished along the banks (Fig. 1). The T_r of each pixel within these polygons was then extracted and the average T_r was calculated and used for further investigations into the effect of spatial temperature on fish assemblages.

2.5.2. Seasonal dynamics of water temperature

Seasonal dynamics of water temperature were investigated using six thermal variables calculated for the T_k of each temperature logger and the gauging station over the four-month period: (i) minimum T_k, (ii) maximum T_k, (iii) average T_k, (iv) T_k pulse (amplitude; i.e., difference between maximum and minimum T_k), (v) maximum kinetic rate of thermal heating (maximum value of the temperature difference per hour), and (vi) maximum kinetic rate of thermal cooling (minimum value of the temperature difference per hour; for calculations see Arscott et al., 2001). In addition, two temperature-related metrics of specific relevance to fish were calculated: (vii) cumulative kinetic degree-days (cumulative temperature sum of average daily temperatures over the four-month collection period), and (viii) cumulative kinetic degree-days above 12 °C (for calculations see Wolter, 2007). Because variables (v) and (vi) are strongly affected by sampling intervals, the logger data were averaged to the gauging station sampling interval of 1 h. In order to calculate the degree-day variables, days with no data (e.g., if the logger went dry) were eliminated for all loggers; thus 96 days out of 119 days were used for the calculations. Furthermore, the average T_k was calculated over 24 h of the two TIR survey days and used for further investigations into the effect of the seasonal dynamics of water temperature on fish assemblages.

2.5.3. Fish assemblages

The fish catches were standardized as catch per unit effort, CPUE (fish caught per 100 m) to calculate and compare relative abundance metrics. The CPUE data were log-transformed ($x+1$) prior to analysis. Furthermore, two additional metrics were calculated for each water body fished: (i) total number of species S, and (ii) Shannon's diversity index H, calculated as $-\sum_{i=1}^{S} p_i \ln p_i$, where p_i is the proportion of each species "i" relative to S in the water body.

2.5.4. Statistical analysis

Differences in the seasonal dynamics of water temperature and fish assemblages among the locations studied were analyzed using non-metric multidimensional scaling (NMS), providing between-location (dis)similarity for each group of variables (eight kinetic thermal variables, CPUE of species). Only species with three or more individuals were included in the fish assemblage ordination, because species with only a few individuals provide little reliability when assigning them to groups (McCune et al., 2000). NMS avoids the error produced by the "zero truncation" problem (where the absence of a species from a water body provides no information about how unfavorable the environment is for that species) common to heterogeneous ecological data sets (Clarke, 1993), and is commonly regarded as the most robust, unconstrained ordination method in community ecology (Minchin, 1987). All NMS solutions were calculated using the Sørensen (Bray–Curtis) distance measure and 250 runs of real data with up to 500 iterations to evaluate the stability; 250 Monte Carlo runs with randomized data evaluated the probability ($p<0.05$) that the ordination axes explained more variation than could be expected by chance. One or two-dimensional ordinations with a final stress <10 (highly reliable graphical representation of the data; Clarke, 1993; McCune & Mefford, 2006) were finally used. The axes were rotated, if necessary, to show the maximum amount of variation on the first axis.

Joint plots were constructed to identify environmental factors that might influence the fish assemblage structure. NMS was used in combination with joint plots to ordinate the fish assemblages in the sample space and to evaluate the association between a fish assemblage and the water temperature, in particular. Three temperature variables were used: (i) temperature measured during electro-fishing, (ii) average daily temperature measured with the loggers, and (iii) average temperature derived from the LWIR mosaic, representing the area of the water bodies fished. Nine out of the eleven initial water bodies were used for this analysis because of a loss of loggers in water bodies A and D (Fig. 1).

Quantitative variables were plotted as vector fits against fish assemblage ordinations. Before the analyses, the secondary matrix (environmental variables) was standardized by calculating the zero-unit mean variance ($z' = \frac{x-\overline{x}}{SD}$, where $\overline{x}$ is the mean and SD the standard deviation) within each variable. Pearson's correlation coefficients were used as relative means to compare the strength of correlations between variables and the ordination axis. Mantel's tests were conducted with Monte Carlo simulations (10,000 randomization runs) and the Sørensen distance measure for both matrices (CPUE of species and environmental variables) to evaluate the correspondence (significance) between dissimilarity matrices. A significant correlation would indicate that, for example, thermally similar locations tend to exhibit similar fish assemblages. All statistical analyses were performed using PC-ORD (version 5.01; McCune & Mefford, 2006).

3. Results

3.1. Spatial thermal heterogeneity at the floodplain scale

A distinct variation in surface water extent and surface temperature was detected at the floodplain scale (Fig. 2). At high flow (spring), most water bodies were hydrologically connected, as reflected in the thermal properties (Fig. 2). For example, a side channel was fully connected to the main channel over its entire length (3900 m) during high flow, whereas it was only connected downstream for 1700 m during mean flow (from "a" to "b", Fig. 2). Furthermore, TIR imagery was able to delineate the flooded area. At high flow, both groynes and sand islands were submerged (zone "c" for the latter in Fig. 2) and most of the floodplain ponds were connected (e.g., zone "d" in Fig. 2).

The radiant temperature (IR pixel $n>12\times10^6$) at the floodplain scale (including terrestrial and aquatic habitats) was very variable during the summer survey (mean flow), whereas it was more uniform during the spring survey (high flow) (histograms in Fig. 2). From spring to summer, the average surface temperature and temperature amplitude at the floodplain scale increased by approximately 13.5 °C and 2.5 °C, respectively (histograms in Fig. 2). Two distinct temperature peaks occurred during both surveys (histograms in Fig. 2). A cool peak (aquatic habitats) with an average temperature of 8.5 °C and a warmer peak (terrestrial surfaces, mainly exposed sand) with an average temperature of 25.5 °C in spring (high flow) (histogram 25 March in Fig. 2). In summer (mean flow), one peak reflected the water temperature of the main channel (26.5 °C), and a second peak reflected the water temperature of the side channel, ponds, as well as of mature vegetation patches (28–29 °C, histogram 14 July in Fig. 2). In the side channel (water bodies H–K, Fig. 1), the water temperature increased by 0.6−0.7 °C (spring) and 0.9–1 °C (summer)

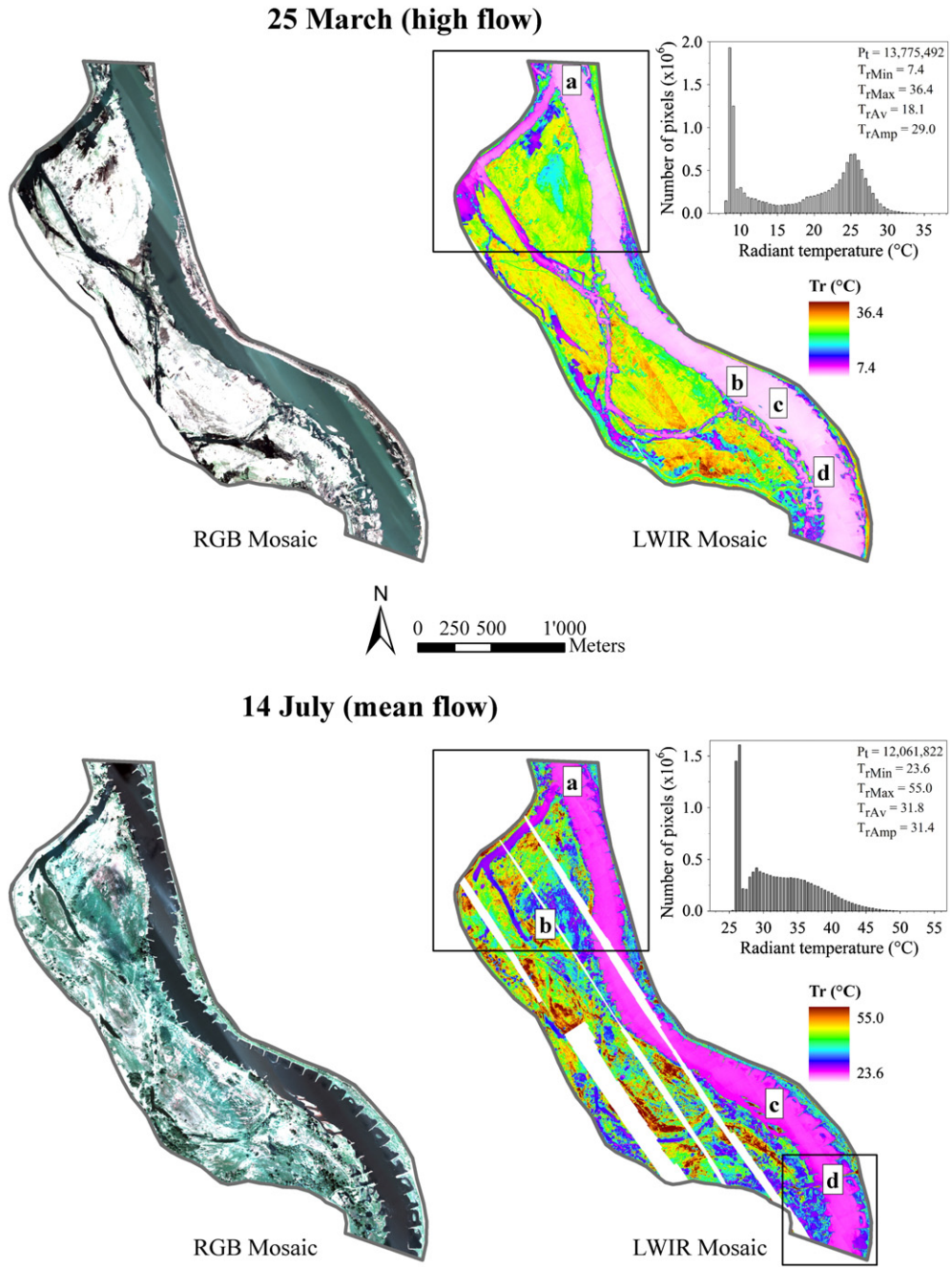

Fig. 2. 16-bit RGB mosaic and corresponding 32-bit LWIR mosaic (spatial distribution of surface radiant temperature, T_r, values per pixel) of the entire floodplain under high and mean flow conditions (missing parts due to sensor and/or GPS malfunctions during the survey). Statistics for each histogram (pixel frequency distribution of radiant temperature over the entire floodplain) include total number of pixels (P_t), minimum radiant temperature (T_{rMin}), maximum radiant temperature (T_{rMax}), average radiant temperature (T_{rAv}), and radiant temperature amplitude (T_{rAmp}). Framed sections are shown in detail in Figs. 3 and 4. Lower case letters indicate interesting zones in respect to hydrological connection and extension of the flooded area (see Section 3.1.).

per 500 m distance, with a sharp increase starting at about 800 m distance from the confluence with the main channel (zones "b" and "e", line plots in Fig. 3). The water temperature ranged between 8.6 and 12.2 °C (spring) and 25.8 and 28.7 °C (summer) in the proximal part of the side channel and between 9.3 and 13.9 °C (spring) and 27.3 and 29.2 °C (summer) in the distal part (histograms in Fig. 3). Mixing processes at the confluence zone between the main channel and the side channel generated sharp water temperature differences over short distances, especially in summer (zones "a" and "d", line plots in Fig. 3). At the terminus of the side channel, where the water depth was shallower, thermal heterogeneity of the water was also high (zones "c" and "f", line plots in Fig. 3). In the main channel (summer), the water temperature was about 2 °C higher in the groyne fields than in the main-channel thalweg, and was similar to the temperature in the connected ponds (Fig. 4).

3.2. Seasonal dynamics of water temperature

At the floodplain scale, the kinetic water temperature (measured by conventional loggers) ranged from 7.3 to 31.6 °C during the recording period (Supplementary Data D). Non-metric multidimensional scaling (NMS), based on eight thermal variables, ordered the water bodies with temperature loggers along a distinct spatial gradient corresponding to decreasing hydrological connectivity (Fig. 5). The main-channel

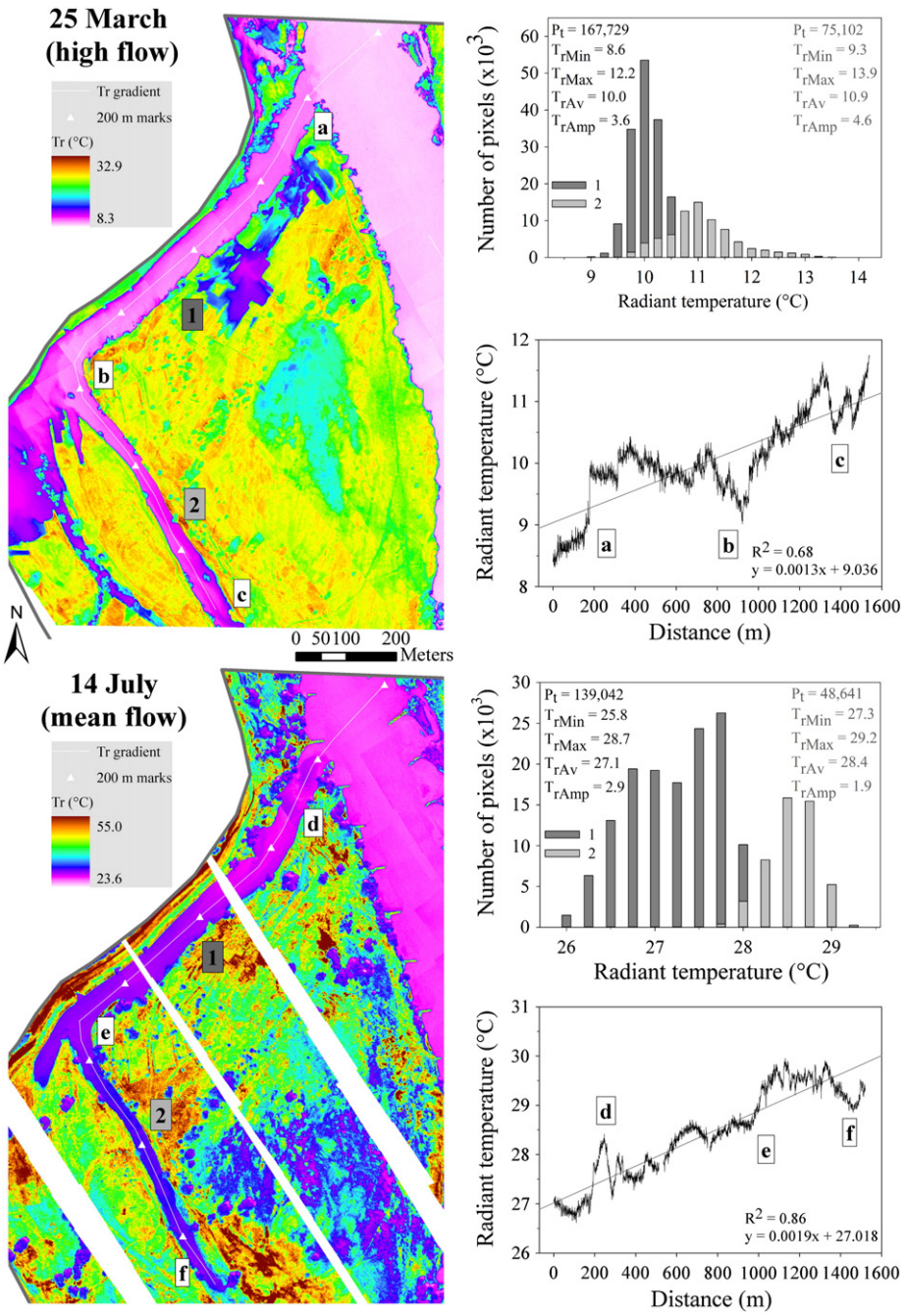

Fig. 3. Spatial distribution of surface radiant temperature (T_r, values per pixel) of a side channel (water bodies H–K, Fig. 1) at high and mean flow. Pixel frequency distributions of water T_r (histograms; see Fig. 2 for abbreviations) and T_r gradients (line plots) are illustrated. Lower case letters indicate interesting zones in the line plots and bordered numbers refer to the histograms (see Section 3.1.).

thalweg (G, Fig. 5) represented the coldest point along the gradient, followed by the water bodies located along the banks of the main channel (# 9, 13, 22), the permanently connected ponds (# 2, 3, 4, 6), the ponds that became isolated at low-mean flow (# 7, 10, 11; with # 5 as an outlier), and the water bodies located in the side channel or in its prolongation (# 14–21) (Fig. 5). Cumulative degree-days and the average and maximum temperatures correlated best with the factor score of the first components of the NMS. The average temperature and cumulative degree-days were strongly correlated with the variables temperature pulse (amplitude) and cumulative degree-days above 12 °C. Furthermore, the maximum temperature was correlated with maximum rate of thermal heating (Spearman's rank correlations, $0.51<r<0.95$, $p<0.05$, $n=20$).

3.3. Fish assemblages

During the spring (high flow) and summer (mean flow) surveys, 1339 and 5192 fish were collected, respectively, representing a total of 26 native species, 24 of them being tolerant or unspecific against high temperatures (Table 3). Barbel (*Barbus barbus*), pikeperch (*Sander lucioperca*), and crucian carp (*Carassius carassius*) were only found during the spring survey, whereas golden loach (*Sabanejewia baltica*), asp (*Aspius aspius*), and European catfish (*Silurus glanis*) were only caught during the summer (Table 3). The total number of fish species per individual water body varied between 7 and 15 (spring) and between 10 and 18 (summer) (Table 4). The dominant species were gudgeon (*Gobio gobio*) and roach (*Rutilus rutilus*) in

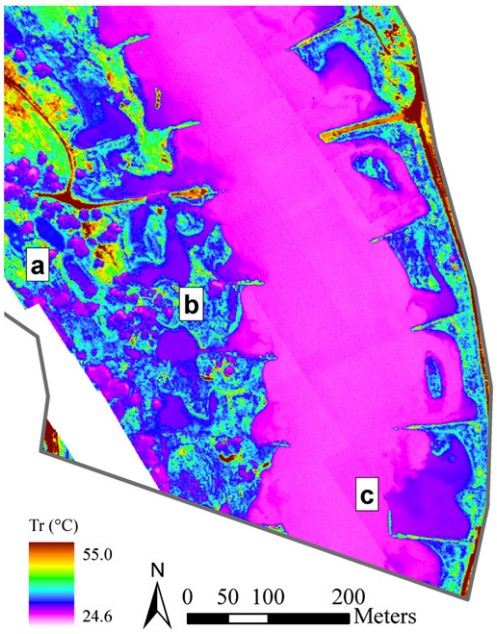

Fig. 4. Spatial distribution of surface radiant temperatures (T_r, values per pixel) during the mean flow of an area including "a" isolated and "b" connected ponds, and "c" the main channel regulated by perpendicular groynes.

spring and spined loach (*Cobitis taenia*) and roach in summer (Table 3). In the side channel the total number of species decreased with increasing distance from the main channel and increasing water temperature. Although the temperature in the distal part of the side channel (water bodies J and especially K, Fig. 1 and histogram in Fig. 3) was already well above the activity level of spring spawning fish providing a substantial incentive (Wolter, 2007), these available warm-water refuges were not adequately used by fish. In contrast to our initial expectations, the temperature refuges were not associated with higher fish densities. However, the proportion of temperature tolerant, i.e. warm-water preferring species was positively correlated to temperature in spring (Table 4). In contrast to our initial hypothesis, the warmest sites did not show the highest proportion of temperature tolerant species during both surveys; however, tolerant and temperature-unspecific fish always summed up to 100% there (Table 4). During summer, the highest proportion of warm-water tolerant fish was found at the main channel sites (Table 4).

Three main fish assemblages were distinguished (Fig. 6): (i) in the side channel (water bodies H–K) the assemblage was dominated by eurytopic species (i.e., species having no flow preference), (ii) in the permanently connected ponds (water bodies B and C) limnophilic species (i.e., species preferring stagnant waters), dominated, and (iii) in the main channel (water bodies A and D–G) the fish assemblage was characterized by rheophilic species (i.e., species preferring flowing waters). The differences between the assemblages were stronger in summer than in spring (Fig. 6).

Kinetic water temperature (spring, summer), dissolved oxygen (spring) and pH (summer) were strongly correlated with the NMS axis (Fig. 6, Table E1 Supplementary Data E). However, Mantel's tests (which evaluate the correspondence, significance, between dissimilarity matrices) showed that during both surveys the relationship was only significant for dissolved oxygen (Table 5). The strongest significant correlation between the categorical environmental variables and fish assemblages was observed for the dominant substrate (Table 5). The fish species most strongly correlated with the primary axis were chub (*Leuciscus cephalus*) and river gudgeon (*Romanogobio belingi*) in spring and chub and rudd (*Scardinius erythrophthalmus*) in summer (Fig. 6, Table E1 Supplementary Data E).

3.3.1. Relationship between fish assemblages and water temperature

In general, the fish assemblages in spring (high flow) exhibited a stronger correlation with temperature than they did in summer (mean flow) (Fig. 7, Table E2 Supplementary Data E). The water body groups and fish species that were most strongly correlated with the two axes were similar to those in the NMS ordination based on 11 water bodies (Fig. 7, Table E2 Supplementary Data E). Significant correlations (Mantel's tests) indicated that thermally similar locations tended to contain similar fish assemblages. Variations in fish assemblage structure correlated best with the daily (24 h data from the survey days) average kinetic temperature in spring and with the average radiant temperature in summer (Table 6, Table E2 Supplementary Data E). Average radiant temperature (derived from the thermal mosaic and representing the area of the water bodies fished) was the only temperature variable that was significantly correlated with differences in fish assemblages between the water bodies in spring and summer (Table 6).

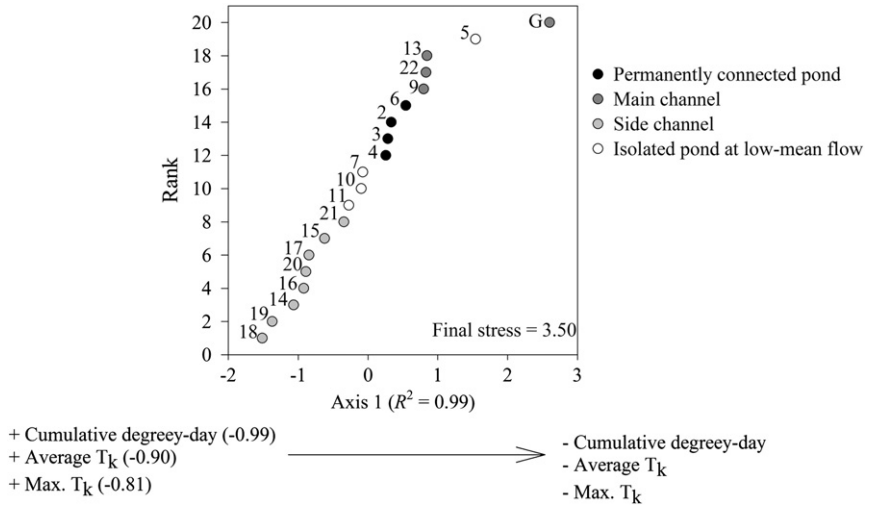

Fig. 5. NMS ordination of the 20 logger locations (see Fig. 1) according to the eight temperature variables calculated for the four-month sampling period. The amount of variation explained by the ordination axis (R^2, $p<0.05$) and the three temperature variables that were most highly correlated with the ordination axis are given in parentheses (Pearson's correlation coefficients). G: gauging station "Frankfurt/Oder" represents the main-channel thalweg.

Table 3
Fish species and total number of specimens caught during spring (high flow) and summer (mean flow); species grouped according to high temperature tolerance, Max. T.: lethal temperature. NA: not available.

Scientific name	Abbreviation	25 March (high flow)	14 July (mean flow)	Max. T. (°C)	Flow preference
Tolerant					
Abramis ballerus (L.)	ABBA	1	2	36	rheophil B
Abramis brama (L.)	ABBR	24	17	36	eurytop
Barbus barbus (L.)	BABA2	2	0	37	rheophil A
Carassius carassius (L.)	CACA	1	0	33–38	limnophil
Leuciscus cephalus (L.)	LECE	59	416	33–36	rheophil A
Rhodeus amarus (Bloch)	RHAM	137	38	37	limnophil
Rutilus rutilus (L.)	RURU	396	1038	33–38	eurytop
Scardinius erythrophthalmus (L.)	SCER	21	164	33–38	limnophil
Silurus glanis (L.)	SIGL	0	6	>35	eurytop
Tinca tinca (L.)	TITI	6	5	37	limnophil
Intolerant					
Gymnocephalus cernuus (L.)	GYCE	7	3	>25	eurytop
Unspecific					
Alburnus alburnus (L.)	ALAL	94	205	30–35	eurytop
Aspius aspius (L.)	ASAS	0	117	30	rheophil B
Barbatula barbatula (L.)	BABA	4	3	29–34	rheophil A
Blicca bjoerkna (L.)	BLBJ	14	319	NA	eurytop
Cobitis taenia (L.)	COTA	40	1163	NA	rheophil B
Esox lucius (L.)	ESLU	57	410	34	eurytop
Gobio gobio (L.)	GOGO	239	38	30	rheophil B
Leuciscus idus (L.)	LEID	11	226	>33	rheophil B
Leuciscus leuciscus (L.)	LELE	10	166	>33	rheophil A
Lota lota (L.)	LOLO	28	52	28-30	rheophil B
Misgurnus fossilis (L.)	MIFO	1	7	NA	limnophil
Perca fluviatilis (L.)	PEFL	164	721	31	eurytop
Romanogobio belingi (Slastenenko)	ROBE	21	4	NA	rheophil A
Sander lucioperca (L.)	SALU	2	0	31	eurytop
NA					
Sabanejewia baltica (Witkowski)	SABA	0	27	NA	rheophil A

4. Discussion

In this study, we quantified thermal heterogeneity during two different flow conditions at the floodplain scale and related it to fish assemblage structure. Based on the thermal properties and the fish assemblage structure, three main habitat types were distinguished: (i) main channel habitats, (ii) connected and isolated ponds, and (iii) side channel habitats. These water bodies were best separated by the thermal variables of cumulative degree-days, and average and maximum temperatures. The strong temperature effect in structuring fish assemblages was also reflected in the high congruency between spatial thermal properties obtained by TIR imagery and fish assemblages surveyed. Therefore, TIR imagery seemed highly suited to capture spatial variation (i.e., extreme values) of water temperature and to indirectly assess fish assemblage structure and habitat use at high spatial resolution over large heterogeneous areas.

Table 4
Main fish population parameters of the 11 water bodies surveyed at high and mean flows (A, D–G: main channel; B, C: permanently connected pond; H–K: side channel; see Fig. 1). CPUE: number of fish caught per 100 m (not log-transformed); *H*: Shannon's diversity index; *S*: total number of species. Kinetic temperature (T_k; same as in Table 2) and relative abundance of high-temperature tolerant and unspecific species in % of the total number of specimens caught (standardized as CPUE).

Sampling day	Variable	Water bodies fished										
		A	B	C[a]	D	E[b]	F	G	H	I	J	K
25 March (high flow)	Length fished (m)	120	300	480	400	80	400	400	300	300	250	250
	CPUE	33	55	73	19	56	30	42	52	21	29	35
	H	1.3	1.3	1.6	2.0	1.7	2.1	1.4	2.0	1.8	1.8	1.5
	S	7	12	14	10	9	15	12	12	11	10	9
	T_k (°C)	8.8	9.2	9.0	7.9	7.9	8.7	8.1	8.8	9.8	10.2	14.0
	Tolerant (%)	64.1	82.5	73.3	36.5	33.3	12.4	14.2	40.4	11.3	34.7	62.1
	Unspecific (%)	35.9	17.5	26.7	63.5	66.7	84.3	85.2	58.3	88.7	65.3	37.9
14 July (mean flow)	Length fished (m)	140	250	70	380	200	460	400	400	330	400	270
	CPUE	275	254	430	306	159	119	176	103	87	58	77
	H	1.9	1.6	1.7	2.1	1.9	2.1	2.1	1.9	1.9	1.9	2.2
	S	15	14	14	18	13	18	17	13	13	11	10
	T_k (°C)	26.0	29.2	29.4	26.8	26.8	26.9	26.7	28.0	28.8	30.5	30.1
	Tolerant (%)	17.7	18.1	13.0	31.1	49.2	52.9	52.5	25.7	24.7	45.3	24.6
	Unspecific (%)	80.8	81.8	86.4	68.7	45.7	46.9	47.5	74.3	74.7	54.7	75.4

[a] Length fished with respect to the water body connected to the main channel under different flow conditions.
[b] Length fished with respect to the emerging bank length of the islands under different flow conditions.

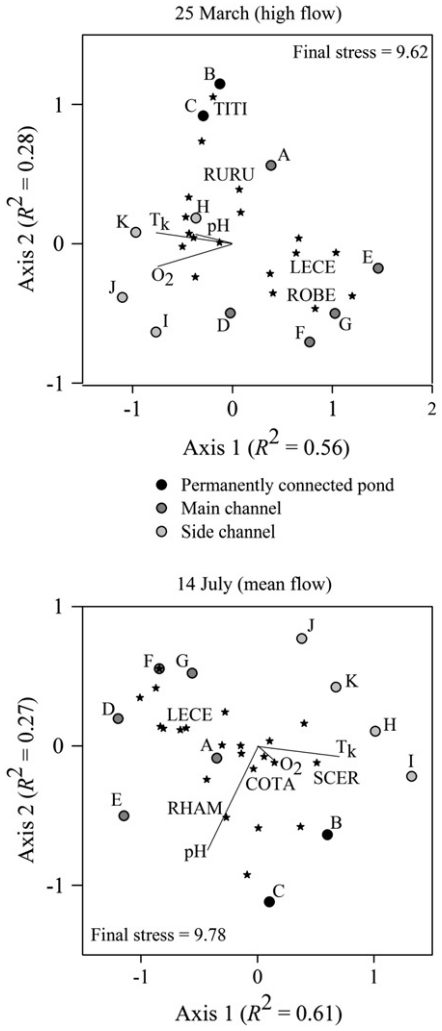

Fig. 6. NMS ordination of the 11 water bodies fished (see Fig. 1) according to their fish assemblages (log-transformed CPUE of species) on the two sampling dates. Dots represent water bodies, stars represent fish species. Joint plot overlays (lines radiating from the centroid) indicate the relative strength and direction of the Pearson's correlations of quantitative environmental variables with the ordination axis (exact values: see Table E1 Supplementary Data E). The amount of variation explained by the ordination axis (R^2, $p<0.05$) and the four fish species (abbreviations: see Table 3) that were most highly correlated with the ordination axis are indicated.

Table 5
Standardized Mantel's statistics (r_m) of the dissimilarity matrices for the categorical and quantitative variables and fish assemblages (log-transformed CPUE of species) in the 11 water bodies fished (see Fig. 1). Significance levels for the Mantel's statistics: *** <0.001, ** <0.01, * <0.05.

Variable	25 March (high flow)	14 July (mean flow)
	r_m (n = 11)	r_m (n = 11)
Categorical		
Sand	0.17	0.14
Silt	0.56***	0.54***
Organic substrate	0.37*	0.50**
Submerged macrophytes	0.05	0.02
Emerged macrophytes	0.32*	0.12
Woody debris	0.11	0.48**
Water depth	0.27*	0.09
Embankment	0.04	0.02
Quantitative		
T_k	0.18	0.36*
O_2	0.29*	−0.24*
pH	−0.04	0.30*

4.1. Spatiotemporal thermal heterogeneity at the floodplain scale

The present study demonstrated that the application of spatially continuous airborne remotely sensed TIR imagery, with a sub-meter resolution, provides a very reliable method for identifying thermal heterogeneity and ecologically relevant warm and cold-water patches (see also Cristea & Burges, 2009; Deitchman & Loheide, 2009; Tonolla et al., 2010; Torgersen et al., 1999, 2001). Furthermore, the in-situ temperature measurements provided critical information on the temporal thermal dynamics of floodplain water bodies (see also Arscott et al., 2001; Malard et al., 2001; Uehlinger et al., 2003). We showed that for a comprehensive thermal characterization of complex river floodplains, and in order to assess thermal patterns that could affect the distribution of biota and ecosystem processes both spatially and temporally, extensive temperature surveys may be required.

In this study, a shifting habitat mosaic (sensu Stanford et al., 2005) of thermal patches, mainly influenced by the degree of hydrological connectivity, was detected across the floodplain. Hydrological connectivity, which determines the extent of flooded surfaces, the emergence and submergence of distinct habitat structures (e.g., sandbars, groynes), and the size of individual patches, was identified as the main factor determining thermal heterogeneity at the floodplain scale. The season (i.e., higher air temperature in summer than in spring) was found to be less relevant for explaining the overall thermal heterogeneity, although it influences the maximum temperature. In summer (mean flow), the Oder floodplain (composed of aquatic and terrestrial habitats) not only exhibited a much higher average temperature but also larger spatial temperature heterogeneity (amplitude) than in spring (high flow). Whereas high surface temperatures in summer are obviously the result of high air temperatures and solar short-wave radiation, differences in the spatial variability were most likely related to the degree of hydrological connectivity, to the water width to depth ratio, and to surface and sub-surface water exchange rates (Malard et al., 2001; Poole et al., 2008; Uehlinger et al., 2003), as well as to vegetation cover (e.g., Tonolla et al., 2010). Similarly, Cardenas et al. (2008), who collected surface temperatures of a stream at base flow and peak flood using a handheld IR camera, found lower thermal heterogeneity under high flow than low flow conditions and stressed that periphyton anchored to the streambed, logs, and partially exposed sandbars significantly contributes to thermal heterogeneity during low flow conditions.

Complex thermal mosaics exhibiting distinct diel dynamics were identified using thermal imagery in braided river floodplains (Tonolla et al., 2010) and alpine terrestrial landscapes (Scherrer & Körner, 2010). The temperature gradient (amplitude) of approximately 30 °C across the entire Oder floodplain (considering both terrestrial and aquatic habitats) during spring (high flow) and summer (mean flow) corresponds well to the thermal range over a distance of several hundred meters across the Roseg and Tagliamento floodplain surfaces at noon in fall (Tonolla et al., 2010). Hydrologically dynamic water bodies such as the main channel provided relatively cool patches (see also Tonolla et al., 2010; Torgersen et al., 1999). In contrast, standing water bodies such as ponds and most of the side channel exhibited larger temperature amplitudes with maximum temperatures of up to 31.5 °C (Supplementary Data D) during hot summer days. The difference of 17 °C between the two temperature peaks (aquatic vs. terrestrial surfaces) across the entire Oder floodplain in spring corresponds well with the spatial variation of peak noon temperatures across the Tagliamento and Roseg floodplains (Tonolla et al., 2010). However, differences between the individual water bodies of the Oder floodplain were smaller than across the Tagliamento (Arscott et al., 2001) and Austrian Danube floodplains (Ward et al., 2002).

The thermal images provided accurate details of a distinct spatial gradient in a side channel and of the thermal effect of groyne fields. Spatial heterogeneity in the side channel (a 5.3 °C difference between the maximum and minimum radiant temperatures, Fig. 3) in spring

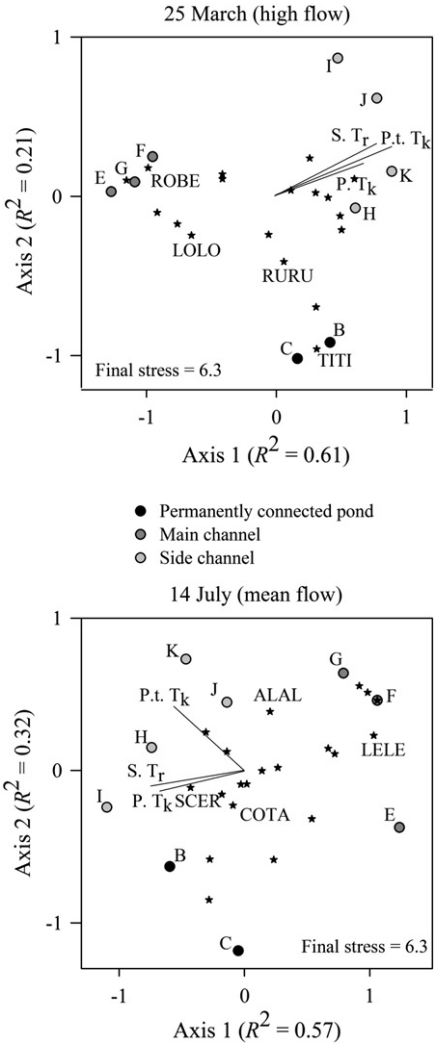

Fig. 7. NMS ordination of the nine water bodies fished with temperature loggers according to their fish assemblages (log-transformed CPUE of species) on the two sampling dates. Dots represent water bodies, stars represent fish species. Joint plot overlays (lines radiating from the centroid) indicate the relative strength and direction of the Pearson's correlations of water temperature with the ordination axis (exact values: see Table E2 Supplementary Data E). P. T_k: "punctual" kinetic temperature measured during electro-fishing, P.t. T_k: "punctual-temporal" average daily kinetic temperature measured by the loggers, S. T_r: "spatial" average radiant temperature derived from the LWIR mosaic (representing the area of the water bodies fished). The amount of variation explained by the ordination axis (R^2, $p<0.05$) and the four fish species (abbreviations: see Table 3) that were most highly correlated with the ordination axis are indicated.

was almost as high as the temporal heterogeneity across the water bodies of the entire floodplain (a 5 °C difference between the maximum kinetic temperatures, Supplementary Data D). The groyne fields in the main channel generated large eddies with very low flowing central habitats fostering a significant temperature increase of up to 2 °C compared to the main channel. This finding emphasizes the utility of airborne remotely sensed TIR imagery as a tool for large-scale spatial temperature mapping and quantification for a more complete ecological understanding from a river-scape perspective.

4.2. Fish assemblages and the effect of thermal patchiness on fish distribution

A total of 26 fish species were caught in this study, which is in agreement with other studies in the lower Oder River (19–26 species; Wolter, 2007; Wolter & Freyhof, 2005) and which can be considered as being representative of the study area.

Table 6
Standardized Mantel's statistic (r_m) of dissimilarity matrices for the temperature variables and fish assemblages (log-transformed CPUE of species) in the nine water bodies fished with temperature loggers (see Fig. 1). Punctual T_k: kinetic temperature measured during electro-fishing; punctual-temporal T_k: average daily kinetic temperature measured by the loggers; spatial T_r: average radiant temperature derived from the LWIR mosaic (representing the area of the water bodies fished). Significance levels for the Mantel's statistics: *** <0.001, ** <0.01, * <0.05.

Variable	25 March (high flow)	14 July (mean flow)
	r_m (n = 9)	r_m (n = 9)
Punctual T_k	0.29	0.37*
Punctual–temporal T_k	0.69***	0.13
Spatial T_r	0.45**	0.37*

We accounted for the impact of thermal stratification on absolute temperature measurements assessed with TIR by using relative thermal patterns. A bias of fish species distribution has to be expected if the surface temperature patterns detected by TIR are stressfully high and fish are actively seeking cold-water refuges. The latter could be excluded in our study given the overall low temperature differences in the water column and the temperature tolerance of the fish species present. The same three water body types, distinguished according to their temperature patterns, could also be separated according to their common fish assemblages. Thermally similar water bodies tended to have similar fish assemblages. However, differentiation between the water body types was clearer in summer (mean flow) than in spring (high flow), whereas, in contrast, the response of the fish to temperature gradients was stronger in spring. These seemingly contradictory findings were a result of the generally lower temperatures that were below the optimum values for fish and the higher temperature homogeneity between the interconnected water bodies under the higher flow conditions in spring.

Many fish species are capable of tracking small differences in water temperature over a short distance and respond to these very small-scale differences by moving to more favorable areas (Mather et al., 2008; Wootton, 1990), which has been particularly well studied in cold-water preferring salmonid fishes (Ebersole et al., 2001; Madej et al., 2006). On the other hand, temperate fishes actively seek out warm thermal refuges to take advantage in terms of activity and metabolism (Meka et al., 2003; Peterson & Rabeni, 1996). Similarly, most fish species in the study area tolerate high water temperatures and were thus expected to migrate into warm-water areas such as the side channel in spring (average temperature of the main channel was 8.5 °C). Increasing temperatures in side waters should induce activity by promoting metabolic rates and triggering spawning. In spring, the side channel showed a distinct thermal gradient with water temperatures up to 5.5 °C warmer than in the main channel. Within the side channel sites, the initial hypothesis that fish, as ectotherms, strongly respond to this pattern of increasing temperatures was well confirmed by both fish densities (CPUE) and relative proportions of warm-water fish species in spring, even though the total number of fish species decreased with increasing distance from the main channel. Despite this available temperature gradient, much higher fish densities and species numbers were found in main channel and backwater habitats. Therefore, it must be concluded that most fish overwinter in the main channel and deep areas along the river banks where temperatures stay low through early spring. Accordingly, species with low temperature thresholds for activity may be able to locate and occupy the first available patches of water with higher temperatures. For example, Wolter (2007) found that the temperature increase in March in the Oder River only promoted the spawning of perch, whereas other species did not substantially benefit from this early warming. The delay in response of fish distribution to the strong thermal gradient recorded in spring has not been observed in other studies. Further investigations of this phenomenon could potentially use TIR imagery to assess shifts in the thermal mosaic of complex riverscapes

to generate hypotheses about fish assemblage response and potential time lags in dispersal.

4.3. Outlook

Temperature drives the major life history traits of fishes (Buisson et al., 2008; Jonsson & Jonsson, 2009; McCullough et al., 2009; Pörtner & Farrell, 2008; Wolter, 2007), is pivotal for floodplain animals such as pond-breeding amphibians by determining their reproductive success and body size (Indermaur et al., 2010; McMenamin et al., 2008), influences community structure, abundance and the emergence of many invertebrates (Durance & Ormerod, 2007; Mouthon & Daufresne, 2006; Richter et al., 2008), and controls key ecosystem processes such as organic matter decomposition as well as soil and sediment respiration (Döring et al., 2011; Langhans et al., 2008).

High resolution TIR imagery provides a unique opportunity to quantify and study thermal heterogeneity at spatial scales relevant to ecosystem processes and biota distribution in entire ecosystems. TIR imagery can be used to identify critical habitats such as cold and warm-water refuges, groundwater upwelling areas, and confluence and mixing areas. All these areas may become critical bottlenecks during periods of low flow or critical temperatures, and thus, relevant management and conservation issues due to the predicted temperature increases and changes in discharge and seasonality of precipitation resulting from global climate change. Furthermore, high resolution TIR imagery may facilitate addressing research questions concerning the effect of river regulation (e.g., groyne fields), water abstraction, and industrial water discharge on the thermal regimes of rivers.

For the successful conservation and restoration of river floodplains we need to understand how the spatiotemporal thermal heterogeneity, and the physical factors that generate it (like inundation dynamics), govern species diversity and ecosystem processes at multiple spatial scales. We encourage the inclusion of terrestrial habitats as well as the vertical and temporal components (see Tonolla et al., 2010) of the temperature regime in future studies of thermal heterogeneity and the temperature regime of river floodplains. Extending the spatial and temporal scales may complicate the interpretation of TIR images due to the varied effects of differing surface materials and atmospheric conditions. However, we may greatly benefit from viewing the entire thermal landscape of rivers, laterally, longitudinally, vertically, and temporally.

The thermal IR images might also assist scientists to more effectively translate conservation and restoration strategies into management and policy by providing a visual representation of habitat heterogeneity rather than by abstract statistical or graphical representations. The method itself is an important survey tool crucial for conservation and restoration planning in complex landscapes such as large floodplain river systems.

Acknowledgments

The authors are especially indebted to the generous field support provided by C. Schomaker and our electro-fishing field crew (J. Hallermann, A. Türck, A. Weber, and H. Zwadlo,). We would like to thank M. S. Lorang for an editorial review and insightful comments on an early stage of the manuscript. Furthermore, we acknowledge the pilot of the Cessna, C. Lindemann, for his skills and helpfulness during the remote sensing flights. In addition, we thank Christian Torgersen as well as two anonymous reviewers for constructive criticism and valuable comments and suggestions that helped to improve the manuscript.

Appendix A. Supplementary data

Supplementary data to this article can be found online at http://dx.doi.org/10.1016/j.rse.2012.07.014.

References

Andrews, B. J., Cardenas, M. B., & Bennett, P. C. (2011). Analysis of turbulent non-isothermal mixing between a jet and cooler ambient water using thermal imagery. *Geochemistry, Geophysics, Geosystems*, *12*, Q07022.

Arscott, D. B., Tockner, K., & Ward, J. V. (2001). Thermal heterogeneity along a braided floodplain river (Tagliamento River, northeastern Italy). *Canadian Journal of Fisheries and Aquatic Sciences*, *58*, 2359–2373.

Bischoff, A. (2002). *Juvenile fish recruitment in the large lowland River Oder: Assessing the Role of physical factors and habitat availability*. Aachen: Shaker Verlag.

Bischoff, A., & Wolter, C. (2001). The flood of the century on the River Oder: Effects on the 0+ fish community and implications for flood plain restoration. *Regulated Rivers: Research & Management*, *17*, 171–190.

Buisson, L., Blanc, L., & Grenouillet, G. (2008). Modelling stream fish species distribution in a river network: The relative effects of temperature versus physical factors. *Ecology of Freshwater Fish*, *17*, 244–257.

Caissie, D. (2006). The thermal regime of rivers: A review. *Freshwater Biology*, *51*, 1389–1406.

Cardenas, M. B., Harvey, J. W., Packman, A. I., & Scott, D. T. (2008). Ground-based thermography of fluvial systems at low and high discharge reveals potential complex thermal heterogeneity driven by flow variation and bioroughness. *Hydrological Processes*, *22*, 980–986.

Cardenas, M. B., Neale, C. M. U., Jaworowski, C., & Heasler, H. (2011). High-resolution mapping of river-hydrothermal water mixing: Yellowstone National Park. *International Journal of Remote Sensing*, *32*, 2765–2777.

Clarke, K. R. (1993). Non-parametric analyses of changes in community structure. *Australian Journal of Ecology*, *18*, 117–143.

Cristea, N. C., & Burges, S. J. (2009). Use of thermal infrared imagery to complement monitoring and modeling of spatial stream temperatures. *Journal of Hydrologic Engineering*, *14*, 1080–1090.

Cuenca, J., & Sobrino, J. A. (2004). Experimental measurements for studying angular and spectral variation of thermal infrared emissivity. *Applied Optics*, *43*, 4598–4602.

Deitchman, R. S., & Loheide, S. P. (2009). Ground-based thermal imaging of groundwater flow processes at the seepage face. *Geophysical Research Letters*, *36*, L14401.

Dohle, W., Bornkamm, R., & Weigmann, G. (1999). Das Untere Odertal: Auswirkungen der periodischen Überschwemmungen auf Biozönosen und Arten. *Limnologie Aktuell*, *Vol. 9*, Stuttgart: Schweizerbart'sche Verlagsbuchhandlung.

Döring, M., Uehlinger, U., Ackermann, T., Woodtli, M., & Tockner, K. (2011). Spatiotemporal heterogeneity of soil and sediment respiration in a river-floodplain mosaic (Tagliamento, NE Italy). *Freshwater Biology*, *56*, 1297–1311.

Dunckel, A. E., Cardenas, M. B., Sawyer, A. H., & Bennett, P. C. (2009). High-resolution in-situ thermal imaging of microbial mats at El Tatio Geyser, Chile shows coupling between community color and temperature. *Geophysical Research Letters*, *36*, L23403.

Durance, I., & Ormerod, S. J. (2007). Climate change effects on upland stream macroinvertebrates over a 25-year period. *Global Change Biology*, *13*, 942–957.

Ebersole, J. L., Liss, W. J., & Frissell, C. A. (2001). Relationship between stream temperature, thermal refugia, and rainbow trout (*Oncorhynchus mykiss*) abundance in arid-land streams, northwestern United States. *Ecology of Freshwater Fish*, *10*, 1–11.

Faux, R. N., Maus, P., Lachowsky, H., Torgersen, C. E., & Boyd, M. S. (2001). *New Approaches for Monitoring Stream Temperature: Airborne Thermal Infrared Remote Sensing*. Inventory and monitoring project report, integration of remote sensing, Remote sensing applications center, USDA Forest service engineering.

Goetz, S. J., Gardiner, N., & Viers, J. H. (2008). Applications of remote sensing to monitoring freshwater and estuarine systems. *Remote Sensing of Environment*, *112*, 3993–4166 (special issue containing 15 articles).

Grift, R. E., Buijse, A. D., Van Densen, W. L. T., Machiels, M. A. M., Kranenbarg, J., Klein Breteler, J. G. P., et al. (2003). Suitable habitats for 0-group fish in rehabilitated floodplains along the lower River Rhine. *River Research and Applications*, *19*, 353–374.

Handcock, R. N., Gillespie, A. R., Cherkauer, K. A., Kay, J. E., Burges, S. J., & Kampf, S. K. (2006). Accuracy and uncertainty of thermal-infrared remote sensing of stream temperatures at multiple spatial scales. *Remote Sensing of Environment*, *100*, 427–440.

Handcock, R. N., Torgersen, C. E., Cherkauer, K. A., Gillespie, A. R., Tockner, K., Faux, R., et al. (2012). Thermal infrared remote sensing of water temperature in riverine landscapes. In P. Carbonneau, & H. Piégay (Eds.), *Fluvial Remote Sensing for Science and Management* (pp. 85–113). New York: John Wiley & Sons (Chapter 5, First Edition).

Indermaur, L., Schmidt, B. R., Tockner, K., & Schaub, M. (2010). Spatial variation in abiotic and biotic factors in a floodplain determine anuran body size and growth rate at metamorphosis. *Oecologia*, *163*, 637–649.

Johnson, L. B., & Host, G. E. (2010). Recent developments in landscape approaches for the study of aquatic ecosystems. *Journal of the North American Benthological Society*, *29*, 41–66.

Jonsson, B., & Jonsson, N. (2009). A review of the likely effects of climate change on anadromous Atlantic Salmon *Salmo salar* and brown trout *Salmo trutta*, with particular reference to water temperature and flow. *Journal of Fish Biology*, *75*, 2381–2447.

Kay, J. E., Kampf, S. K., Handcock, R. N., Cherkauer, K. A., Gillespie, A. R., & Burges, S. J. (2005). Accuracy of lake and stream temperatures estimated from thermal infrared images. *Journal of the American Water Resources Association*, *41*, 1161–1175.

Langhans, S. D., Tiegs, S. D., Gessner, M., & Tockner, K. (2008). Leaf decomposition heterogeneity across a riverine floodplain mosaic. *Aquatic Sciences*, *70*, 337–346.

Lillesand, T. M., Kiefer, R. W., & Chipman, J. W. (2008). Multispectral, thermal, and hyperspectral sensing. In T. M. Lillesand, R. W. Kiefer, & J. W. Chipman (Eds.), *Remote Sensing and Image Interpretation* (pp. 325–391). New York: John Wiley & Sons.

Loheide, S. P., & Gorelick, S. M. (2006). Quantifying stream-aquifer interactions through analysis of remotely sensed thermographic profiles and in-situ temperature histories. *Environmental Science and Technology*, *40*, 3336–3341.

LUABB (1998). Landesumweltamt Brandenburg: das Sommerhochwasser an der Oder 1997. *Studien und Tagungsberichte*, *16*.

Madej, M. A., Currens, C., Ozaki, V., Yee, J., & Anderson, D. G. (2006). Assessing possible thermal rearing restrictions for juvenile coho salmon (*Oncorhynchus kisutch*) through thermal infrared imaging and in-stream monitoring, Redwood Creek, California. *Canadian Journal of Fisheries and Aquatic Sciences*, *63*, 1384–1396.

Magnuson, J. J., Crowder, L. B., & Medvick, P. A. (1979). Temperature as an ecological resource. *American Zoologist*, *19*, 331–343.

Malard, F., Mangin, A., Uehlinger, U., & Ward, J. V. (2001). Thermal heterogeneity in the hyporheic zone of a glacial floodplain. *Canadian Journal of Fisheries and Aquatic Sciences*, *58*, 1319–1335.

Marcus, W. A., & Fonstad, M. A. (2008). Optical remote mapping of rivers at sub-meter resolutions and watershed extents. *Earth Surface Processes and Landforms*, *33*, 4–24.

Mather, M. E., Parrish, D. L., Campbell, C. A., McMenemy, J. R., & Smith, J. M. (2008). Summer temperature variation and implications for juvenile Atlantic salmon. *Hydrobiologia*, *603*, 183–196.

McCullough, D. A., Bartholow, J. M., Jager, H. I., Beschta, R. L., Cheslak, E. F., Deas, M. L., et al. (2009). Research in thermal biology: burning questions for coldwater stream fishes. *Reviews in Fisheries Science*, *17*, 90–115.

McCune, B., & Mefford, M. J. (2006). *PC-ORD. Multivariate analysis of ecological data.* Gleneden Beach, Oregon, USA: MjM Software Version 5.

McCune, B., Rosentreter, R., Ponzetti, J. M., & Shaw, D. C. (2000). Epiphyte habitats in an old conifer forest in western Washington, USA. *Bryologist*, *103*, 417–427.

McMenamin, S. K., Hadly, E. A., & Wright, C. K. (2008). Climatic change and wetland desiccation cause amphibian decline in Yellowstone National Park. *Proceedings of the National Academy of Sciences*, *105*, 16988–16993.

Meka, J. M., Knudsen, E. E., Douglas, D. C., & Benter, R. B. (2003). Variable migratory patterns of different adult rainbow trout life history types in a southwest Alaska watershed. *Transactions of the American Fisheries Society*, *132*, 717–732.

Mertes, L. A. K. (2002). Remote sensing of riverine landscapes. *Freshwater Biology*, *47*, 799–816.

Minchin, P. R. (1987). An evaluation of relative robustness of techniques for ecological ordinations. *Vegetatio*, *69*, 89–107.

MODIS (2011). Moderate Resolution Imaging Spectrometer: Emissivity Library. University of California, Santa Barbara, CA, USA. http://g.icess.ucsb.edu/modis/EMIS/html/em.html (last accessed 30th November 2011).

Mouthon, J., & Daufresne, M. (2006). Effects of the 2003 heatwave and climatic warming on mollusc communities of the Saône: A large lowland river and of its two main tributaries (France). *Global Change Biology*, *12*, 441–449.

Peterson, J. T., & Rabeni, C. F. (1996). Natural thermal refugia for temperate warmwater stream fishes. *North American Journal of Fisheries Management*, *16*, 738–746.

Poole, G. C., O'Daniel, S. J., Jones, K. L., Woessner, W. W., Bernhardt, E. S., Helton, A. M., et al. (2008). Hydrologic spiralling: The role of multiple interactive flow paths in stream ecosystems. *River Research and Applications*, *24*, 1018–1031.

Pörtner, H. O., & Farrell, A. P. (2008). Physiology and climate change. *Science*, *322*, 690–692.

Pusch, M., Andersen, H. E., Bäthe, J., Behrendt, H., Fischer, H., Friberg, N., et al. (2009). Rivers of the central European highlands and plains. In K. Tockner, U. Uehlinger, & C. T. Robinson (Eds.), *Rivers of Europe* (pp. 525–576). Amsterdam: Academic Press.

Richter, O., Suhling, F., Mueller, O., & Kern, D. (2008). A model for predicting the emergence of dragonflies in a changing climate. *Freshwater Biology*, *53*, 1868–1880.

Scherrer, D., & Körner, C. (2010). Infra-red thermometry of alpine landscapes challenges climatic warming projections. *Global Change Biology*, *16*, 2602–2613.

Schomaker, C., & Wolter, C. (2011). The contribution of long-term isolated water bodies to floodplain fish diversity. *Freshwater Biology*, *56*, 1469–1480.

Shuman, C. S., & Ambrose, R. F. (2003). A comparison of remote sensing and ground-based methods for monitoring restoration success. *Restoration Ecology*, *11*, 325–333.

Stanford, J. A., Lorang, M. S., & Hauer, F. R. (2005). The shifting habitat mosaic of river ecosystems. *Verhandlungen der internationalen Vereinigung für Theoretische und Angewandte Limnologie*, *29*, 123–136.

Tiffan, K. F., Kock, T. J., Connor, W. P., Steinhorst, R. K., & Rondorf, D. W. (2009). Behavioural thermoregulation by subyearling fall (autumn) Chinook salmon *Oncorhynchus tshawytscha* in a reservoir. *Journal of Fish Biology*, *74*, 1562–1579.

Tockner, K., & Stanford, J. A. (2002). Riverine floodplains: Present state and future trends. *Environmental Conservation*, *29*, 308–330.

Tonolla, D., Acuña, V., Uehlinger, U., Frank, T., & Tockner, K. (2010). Thermal heterogeneity in river floodplains. *Ecosystems*, *13*, 727–740.

Torgersen, C. E., Baxter, C. V., Li, H. W., & McIntosh, B. A. (2006). Landscape influences on longitudinal patterns of river fishes: spatially continuous analysis of fish-habitat relationships. In R. M. Hughes, L. Wang, & P. W. Seelbach (Eds.), *Landscape Influences on Stream Habitats and Biological Assemblages. American Fisheries Society, Symposium 48, Bethesda, Maryland, USA.* (pp. 473–492).

Torgersen, C. E., Faux, R. N., McIntosh, B. A., Poage, N. J., & Norton, D. J. (2001). Airborne thermal remote sensing for water temperature assessment in rivers and streams. *Remote Sensing of Environment*, *76*, 386–398.

Torgersen, C. E., Price, D. M., Li, H. W., & McIntosh, B. A. (1999). Multiscale thermal refugia and stream unit associations of chinook salmon in northeastern Oregon. *Ecological Applications*, *9*, 301–319.

Uehlinger, U., Malard, F., & Ward, J. V. (2003). Thermal patterns in the surface waters of a glacial river corridor (Val Roseg, Switzerland). *Freshwater Biology*, *48*, 284–300.

Van den Brink, F. W. B., Van der Velde, G., Buijse, A. D., & Klink, A. G. (1996). Biodiversity in the lower Rhine and Meuse river-floodplains: its significance for ecological river management. *Netherlands Journal of Aquatic Ecology*, *30*, 129–149.

Ward, J. V. (1998). Riverine landscapes: Biodiversity patterns, disturbance regimes, and aquatic conservation. *Biological Conservation*, *83*, 269–278.

Ward, J. V., Tockner, K., Arscott, D. B., & Claret, C. (2002). Riverine landscape diversity. *Freshwater Biology*, *47*, 517–539.

Webb, B. W. (1996). Trends in stream and river temperature. *Hydrological Processes*, *10*, 205–226.

Welcomme, R. L. (1979). *Fisheries Ecology of Floodplain Rivers.* London: Longman.

Wolter, C. (2007). Temperature influence on the fish assemblage structure in a large lowland river, the lower Oder River, Germany. *Ecology of Freshwater Fish*, *16*, 493–503.

Wolter, C., & Freyhof, J. (2005). Die Fischbesiedelung des Oder-Einzugsgebietes. *Nationalpark-Jahrbuch Unteres Odertal*, 37–63.

Wootton, R. J. (1990). *Ecology of Teleost Fishes.* London: Chapman & Hall.